energies

MDPI

Article

The Electrochemical Commercial Vehicle (ECCV) Platform

Max Johansson [1,*], Arnaud Contet [2], Olof Erlandsson [2], Robin Holmbom [1], Erik Höckerdal [3], Oskar Lind Jonsson [1], Daniel Jung [1] and Lars Eriksson [1,*]

1 Department of Electrical Engineering, Linköping University, SE 581 83 Linköping, Sweden; robin.holmbom@liu.se (R.H.); oskar.lind.jonsson@liu.se (O.L.J.); daniel.jung@liu.se (D.J.)
2 TitanX Engine Cooling AB, SE 294 71 Sölvesborg, Sweden; arnaud.contet@titanx.com (A.C.); olof.erlandsson@titanx.com (O.E.)
3 Scania CV AB, SE 151 48 Södertalje, Sweden; erik.hockerdal@scania.com
* Correspondence: max.johansson@liu.se (M.J.); lars.eriksson@liu.se (L.E.)

Abstract: Several technological challenges delay the adoption of electrified powertrains in the heavy-duty transport sector. For fuel-cell hybrid electric trucks, key issues include slow cold start, reduced cooling power during high ambient temperatures, and uncertainties regarding durability. In addition, the engineers must handle the complexity of the system. In this article, a Matlab/Simulink library is introduced, which has been developed to aid engineers in the design and optimization of energy management systems and strategies of this complex system that consider mechanical, electrochemical, and thermal energy flows. The library is introduced through five example vehicle models, and through case studies that highlight the various kinds of analysis that can be performed using the provided models. All library code is open source, open for commercial use, and runs in Matlab/Simulink without any need for external libraries.

Keywords: electric vehicles; energy management; thermal management

Citation: Johansson, M.; Contet, A.; Erlandsson, O.; Holmbom, R.; Höckerdal, E.; Jonsson, O.L.; Jung, D.; Eriksson, L. The Electrochemical Commercial Vehicle (ECCV) Platform. *Energies* **2024**, *17*, 1742. https://doi.org/10.3390/en17071742

Academic Editor: Fangming Jiang

Received: 5 February 2024
Revised: 12 March 2024
Accepted: 27 March 2024
Published: 4 April 2024

1. Introduction

In 2017, the transport sector accounted for 31% of the global energy consumption [1], and a significant portion of the total freight was hauled by heavy-duty (HD) vehicles. According to statistics from Germany, over 95% of all freight is moved by vehicles that surpass a weight of 12.5 tons [2]. Class 8 trucks (classified as vehicles weighing over 15 tons) travel in the range of 160–800 km per day (averaging about 96,500 km per year) [3], and the US Department of Energy projects this figure to increase by 80% from 2010 to 2050 [4]. The heavy-duty transport industry performs a crucial function in society, and the dependence on heavy-duty vehicles is projected to increase. As extensive reductions in emissions are required across all industries [2], both industry and academia are looking towards new technologies in order to meet future demands on road vehicles.

One path towards reducing the emissions from the transport industry is through electrification, and heavy-duty (HD) fuel-cell hybrid electric vehicles (FCHEVs) are considered as a solution in transitioning to clean energy, where the possibility of rapid refueling and the high energy density of hydrogen provides some advantages over pure battery vehicles [1,5].

Currently, several HD-FCHEV research initiatives and pilot projects are in motion. Some well-known are the Hyundai Xcient, Mercedes-Benz GenH2, and Nikola Motors Tre [6]. Projections on HD-FCHEVs are also positive. In 2019, there were approximately 400 fuel cell (FC) trucks out on the roads, out of 10,000 total FCHEVs, and some projections say that number will reach 500,000 FC trucks by 2030, and 15–20 million by 2050 [1].

However, there are several disadvantages to fuel cell systems that need to be addressed before widespread adoption. Some of the main issues are the high production cost, insufficient refueling infrastructure, safety concerns relating to pressurized hydrogen gas, cold start issues, and insufficient development of energy management strategies (EMSs) [1,7,8].

Poor thermal management can cause cell degradation due to both temperature and humidity cycling [7], but degradation mechanisms tend to not be considered in studies on EMS systems [9]. Most studies on EMS focus on single objectives, such as minimizing energy consumption, cost of operation, or emissions [10]. Furthermore, cold ambient temperatures can have severe negative effects on hydrogen consumption [11].

Thermal systems and their management in battery electric vehicles (BEVs) and FCHEVs are more complex than for conventional vehicles and the industry has a clear need for systematic design tools for their architectural layout, dimensioning, and control. The thermal systems must handle bidirectional heat flows, ambient conditions ranging from subzero to high temperatures, and highly dynamic load conditions. The cabin, battery pack, fuel cell stacks, power electronics, and electric machines form a network of producers and consumers of heat, which require a complex thermal system layout. However, the complexity also generates opportunities. Intelligent control systems could increase fuel efficiency and reduce thermal cycling by transporting heat from producers to consumers as the need arises.

The dynamic demands on intelligent thermal management systems require that control aspects are considered early in the design. For these purposes, a modular platform-based approach has been developed to enable robust design and fast evaluation of thermal systems. Model-based methodologies play an indispensable role in tackling this challenging task [12,13], as models may alleviate the need for costly experimental testing and calibration, system integration and requirement testing at the early design phase, and shorten the time to market. The electrochemical commercial vehicle (ECCV) platform proposed and developed in this article fulfills the specifications above: the models are control-oriented, modular, dynamic, and lightweight. The ECCV platform can serve as a singular source for design, optimization, and control development for intelligent energy & thermal management systems for electrified commercial vehicles, and as an enabler of interdisciplinary collaboration in the automotive research community.

Full vehicle simulators like the ECCV platform exist on a spectrum of complexity. There are tools like FASTSim [14], where vehicles are characterized by a few important parameters and where velocity profiles are fixed. The tool is simple but robust, but since dynamics are not considered, it is unsuitable for control design. A widely used simulation tool in the automotive industry is the proprietary software GT-SUITE [15], which can simulate one-dimensional differential equations and achieves great accuracy at the cost of computational complexity. In [16], the authors coupled a Matlab/Simulink vehicle model to a thermal model in GT-SUITE. The vehicle simulation tool provided in [17] is similar to the ECCV platform in that it is based on Matlab/Simulink, but differs in the simulation approach. The provided tool uses mainly a backward approach, where the vehicle state is calculated from a fixed velocity profile, and no thermal systems are included. The ECCV platform is fully dynamic, using the forward approach, and includes models for the thermal management system. Automotive thermal management systems were modeled in Matlab/Simulink by researchers at the National Renewable Energy Laboratory (NREL) [18–22], where one major contribution was the quasi-transient methodology for efficient simulation of coolant and refrigerant systems where flow reversals may occur. In the ECCV platform, the coolant flow path is modeled by feedback of pressure information, as described in later sections.

The main contribution to the scientific community is the compiled simulation platform, which is provided as open source and downloadable from www.fs.isy.liu.se/Software (accessed on 4 February 2024). An interested user can also request to be invited to the git repository used for development, instructions are given on the download page. The platform has been developed in several research projects together with industrial partners, and they have monitored the system and component development so that the vehicle model will be relevant to their needs. The models and library are component-based and the interface designs for the connections between components in different domains enable the system to be extended and modified. This is demonstrated in this paper by a sequence of examples that have increasing levels of complexity in the models. A model built from the simulation platform and library has also served as a basis for an industrially motivated control benchmark competition problem called "ECCV Control Benchmark for Sustainable Transport" at the IFAC 2023 World Congress in Kyoto Japan.

2. Challenges, Aim and Method

Fuel cell electric vehicles are complex to manage, control, and optimize. To handle this complex system with systematic methods a model-based approach is necessary [23], as a natural consequence, system and component models are therefore also needed. However, it requires significant resources to develop a simulation model that is of industrial relevance. The OEMs have in-house models but these often contain elements covered by Intellectual Property Rights (IPR) that hinder sharing with a larger part of the research community. The aim here is to provide a generic simulation platform that can be used by researchers and engineers who want to analyze energy consumption and flows in vehicle systems and develop control strategies that are of industrial relevance. The platform also aims to be open and documented so it can be shared among stakeholders and those who have a general interest in working on the system without causing IPR problems. This also facilitates the possibility of making fair comparisons between different vehicle configurations and sharing the results, providing an open climate for the exchange of ideas and thus a more rapid progress toward sustainability.

The method used to develop the platform has been to run collaborative projects with industries and universities that identify the important features and aspects of the system and view the challenges both from the research and development perspectives. The platform has its origin in a physics-based heavy-duty conventional diesel truck that was used in a benchmark competition for look-ahead control and planning of the driving of the vehicle on a virtual road with a set of road profiles and ambient conditions. The industries were satisfied with the agreement between the model and the related behaviors of their products, and the research questions that could be addressed by the research community were also relevant to the industries. The diesel-based powertrain was changed to an electric one while building on the validated models for the vehicle, road, and world. In the development, a sequence of projects has contributed with their lessons learned and provided components that have been included in the library, which now provides a flexible platform for electric and fuel cell vehicle simulation.

In the system modeling process, the component models have been identified from the research literature to provide a scientific base for the models and interfaces have been constructed so that they can be integrated into a complete vehicle system model. The components are referenced in the descriptive texts below.

3. Overview of the Platform and Its Components

This section begins with an overview of the ECCV platform structure and interfaces, followed by the specifics of the various types of models that are included. Then, six example vehicle models and case studies are introduced to highlight the capabilities of the ECCV platform. The main focus of the examples is to highlight the energy flows and how different component properties influence the complete system performance. Table 1 shows the notation used in the text and figures below.

Table 1. Notation.

Variable	Description	Variable	Description
W	Mass flow	P	Power
p	Pressure, partial pressure	I	Electrical current
V	Voltage	T	Temperature
T_q	Torque	ω	Angular velocity, flow split fraction

Table 1. *Cont.*

Variable	Description	Variable	Description
F	Force	v	Longitudinal velocity
m	Mass	V	Volume
Q	Heat flow	C_p	Heat capacity
u	System input	α	Road slope

3.1. Library Structure and Model Interfaces

The ECCV platform is a Matlab/Simulink library developed with the purpose of simulating heavy-duty fuel-cell hybrid electric and battery-electric commercial vehicles. In particular, the platform is designed to simulate the flow and interactions between mechanical, electrochemical, and thermal energy. The library structure is shown in Figures A1–A3.

A typical example of how the models interact and send information between components is shown in Figure 1. A compressor provides pressurized air to the fuel cell. Internally, the fuel cell converts hydrogen and oxygen to electrical current and waste heat. The electrical current produced by the fuel cell is consumed in part by its balance of plant components, but mainly by the electric machine (EM), where it is converted to torque and additional waste heat. The torque from the electrical machine is finally converted to a force acting on the truck chassis, that overcomes the losses and builds up kinetic energy. The thermal masses of the fuel cell and electric machine are connected in series to the main coolant circuit.

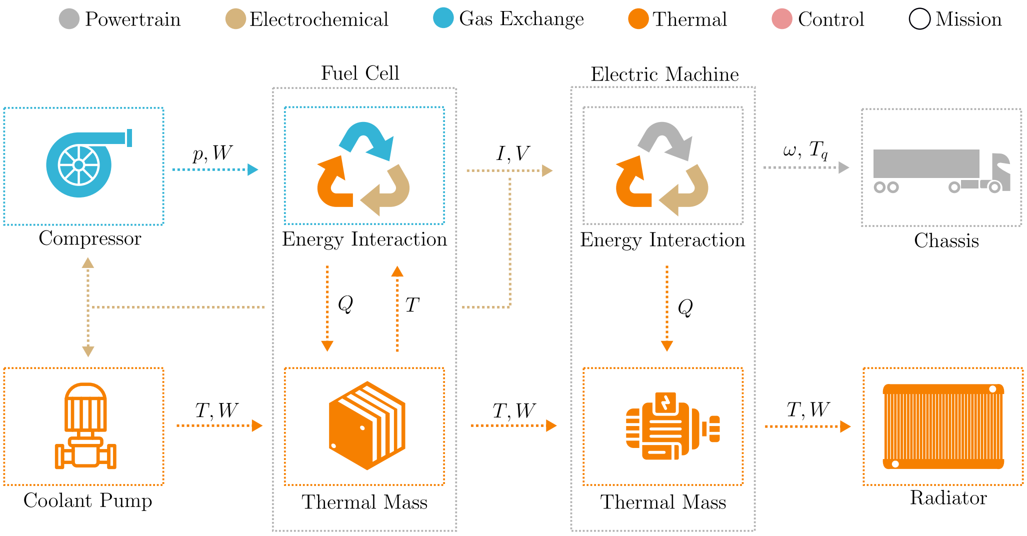

Figure 1. A high-level diagram of how the ECCV platform treats energy interactions, between color-coded domains. The chassis and powertrain with gearboxes and motors are in the mechanical domain. The fuel cell and battery are in the electrochemical domain. The gas flows to and from the fuel cell stack are naturally in the Gas Exchange domain. While, the thermal system has its own domain with thermal masses, radiators and transport in the form of coolant media. To accomplish driving missions it is necessary to have controllers that control various components, like machines, converters, valves and compressors, and these have their own domains.

The library is sectioned into six categories, as indicated by the color scheme shown in the legend at the top of Figure 1. The categories represent physical domains that have guided the component design and the emphasis has been to make the component interfaces general so the components can be scaled or exchanged to represent varying sizes, enabling studies of dimensioning of the system. The details of each category are explained below.

3.1.1. Driving Missions

At a high level, a scenario is specified as a driving mission. It contains an altitude profile, with vehicle speed set points and limits as well as ambient conditions, to also enable high altitudes and hill climbing the NASA troposphere model is implemented. The most important effect is that the road slope has a significant impact on the vehicle velocity. The vehicle model, described below, uses road slope data from the mission to calculate gravitational driving resistance. The mission category also contains tools to import road altitude profiles and the troposphere models that provide ambient conditions based on altitude.

Tests on various roads are an important part of the industrial development process. Engineers and researchers run tests to see that the vehicle and its components can cope with the variations in load that different usage profiles impose on the system. Therefore the platform is prepared to enable an easy change and addition of profile. Additional environmental factors such as wind speed and road temperature planned to be included in the platform.

3.1.2. Powertrain

The powertrain models consist of the chassis, gearbox, and electric machine. The foundation for the chassis model is Newton's second law for acceleration and velocity, which is driven by the force balance between tractive and resistive forces as illustrated in Figure 2. The tractive force comes from the electric machine that is connected to the wheels through a gearbox. The motion-dependent forces that act on the chassis are the rolling, air drag, and gravitational resistance, of which the gravitational resistance is the dominant term in a heavy-duty truck. The model parameters for the chassis and gearbox are taken from a previous truck benchmark problem [24].

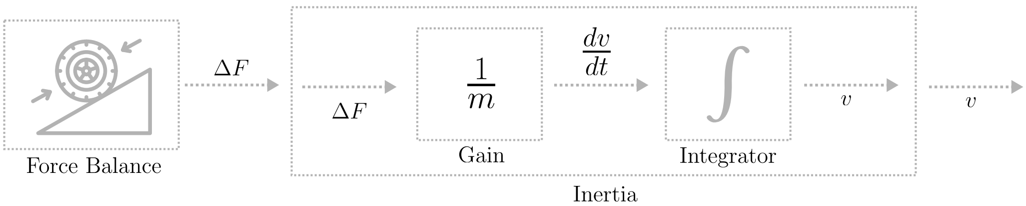

Figure 2. Illustration of Newton's second law, which is the core of the mechanical domain, in the powertrain chassis model. The chassis interacts with the driving missions, like slope and ambient conditions.

3.1.3. Electrochemical

The core models of the electrochemical systems are the battery and the fuel cell. The battery cell currently implemented in the ECCV platform is a Panasonic 18650PF (Eindhoven, The Netherlands), with a nominal capacity of 2.9 Ah. The model is of equivalent circuit type, with five resistor-capacitor circuits in series that approximate a Warburg impedance [25]. The open circuit voltage model is a general functional form [26]. The parameter estimation and model validation were performed on openly distributed pulse-response, slow discharge, and drive-cycle data [27]. For each pulse test, the parameters are estimated by grey-box estimation methods from the Matlab System identification toolbox [28]. The model validation for 25 °C is shown in Figure 3. The experimental data [27] is an automotive drive cycle, appropriately scaled for a single cell, with current and voltage measurements. The figure shows model fit when the ambient temperature is 25 °C, from 100 to 30% stage of charge. The battery pack model is constructed by combining cells in series and parallel, and the DC converter is modeled as a constant efficiency transformer.

A user that has another battery type can easily add new battery cell models either by adjusting the model parameters or by providing a new model function that follows the same function interface.

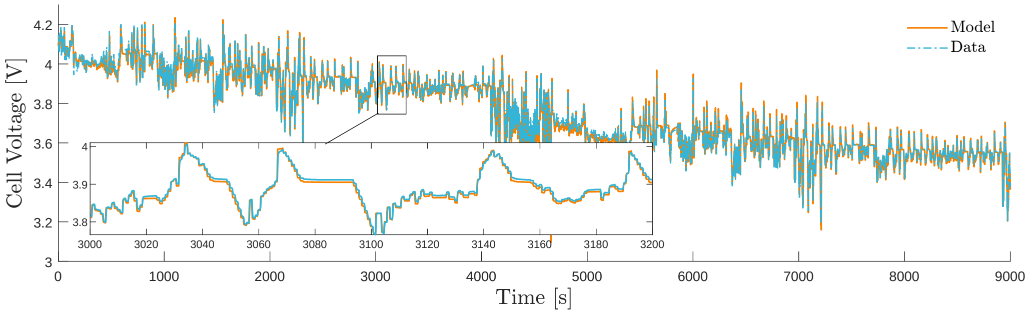

Figure 3. Validation of the battery cell model when it is tested on the dynamic automotive drive cycle data from [27]. The agreement between the model and data is good both with respect to fast dynamics and long-term discharge of energy. The secondary graph shows.

The fuel cell voltage model in the ECCV library is based on multiple terms: open circuit voltage and activation, ohmic, and concentration voltage losses. The losses are dependent on reactant pressures, membrane hydration, and current density using the correlations in [29]. The voltage response for pressures in the range 1–4 bar, a temperature of 80 °C, and relative humidity of approximately 85%, is shown in Figure 4. The figure validates that the model captures the trends in voltage with pressure and current. The resulting power density is shown to the right.

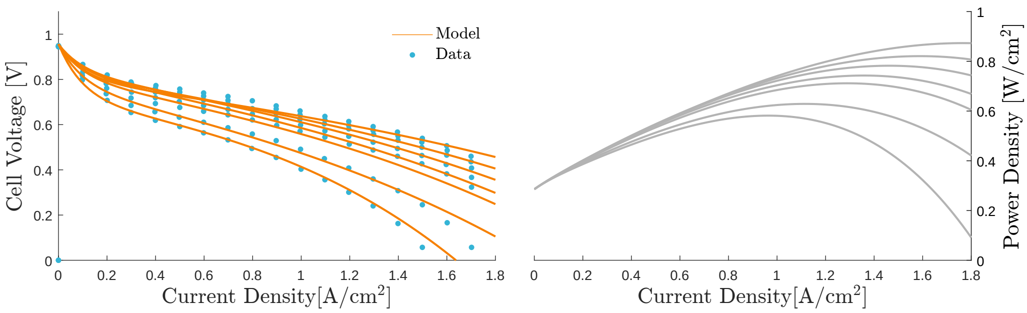

Figure 4. The left graph shows the fuel cell model fit to data [29]. The curves represent anode and cathode pressures evenly spaced between 1 and 3.5 bar. The figure shows that the model can capture variations in pressures and that the maximum power output can be controlled by these variations. The right graph shows the calculated power density.

3.1.4. Gas Exchange

The air and fuel systems are modeled as ideal mixtures of hydrogen, oxygen, water, and nitrogen, where all components are tracked with their individual partial pressures as states in the gas model. Figure 5 shows the typical situation when working with the ECCV gas exchange models. The flow models use upstream and downstream pressures to calculate a flow, and the control volumes use the upstream and downstream flow to calculate pressure, using mass conservation and the ideal gas law.

The flow models use a difference in total pressure to calculate a total convective flow. The mass fractions of the gas composition in the upstream control volume are then used to distribute the flow onto each species. The net flow of each species is integrated by the control volume to provide a partial pressure. Partial pressures are convenient when describing the thermodynamic state for simulation purposes but are not intuitive for users. The library therefore provides tools to convert partial pressures to more familiar descriptions of the state, such as total pressure, relative humidity, and dry gas composition.

Core models of the gas exchange system are the compressor, ejector, and control volumes. The compressor model used in the examples is based on a Mitsubishi TD04 turbocharger. The ellipse compressor model structure [30] is used. It is a generic structure that can describe both choke and surge regions for a compressor and the parameter estimation is performed in the LiuCPGui-toolbox [31] that is based on total least squares curve fitting method [32] of the model parameters to data. The flow and efficiency model fit is shown in Figure 6. The compressor flow model shows the backward implementation of [30] for the surge flow, which is not included in the ECCV library. Instead, the forward approach uses linear extrapolation for compressor flow in the surge region.

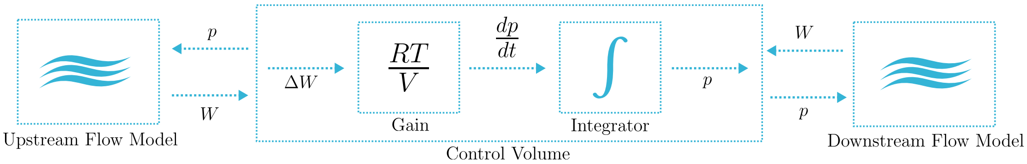

Figure 5. Gas exchange control volume model. The surrounding components determine the mass flows of the gas components and the control volume determines the changes in masses and integrates them into their partial pressures through the ideal gas law, where R is the universal gas constant.

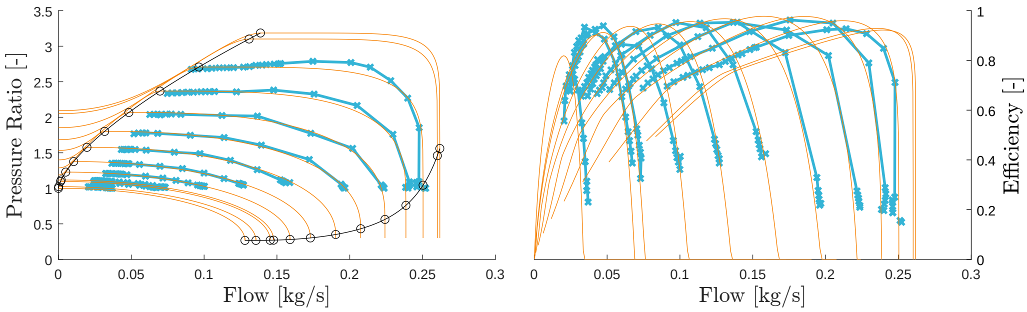

Figure 6. Compressor flow and efficiency map model fit for a Mitsubishi TD04 compressor. Measurement data is given in blue and the model in orange, the left plot shows the flow versus pressure ratio characteristics and the right shows efficiency. The curves represent constant compressor speeds evenly spaced between 60 and 160 krpm.

The ejector is modeled as a compressible flow through a nozzle, and the recirculation ratio is correlated to the pressure ratio over the primary and outlet manifolds. The geometry and data are taken from an ejector designed for 80 kW fuel cell stacks [33,34].

3.1.5. Thermal

For laminar flow in pipes, the correlation of Haussen from [35] is used to calculate average Nusselt numbers and heat transfer coefficients. For some components, the temperature gradients and changes in the coolant fluids are not modeled explicitly but are assumed to be equal to the outflow coolant. In those cases, the heat generated/removed by the component is added/subtracted to the coolant, which results in a temperature increase/decrease. For components with significant thermal inertia, the temperature is modeled according to the diagram in Figure 7. The radiator's overall heat transfer coefficient is modeled using the Effectiveness-NTU approach [35], assuming unmixed cross-flow conditions. The radiator model and its parameters were implemented based on a library provided by TitanX.

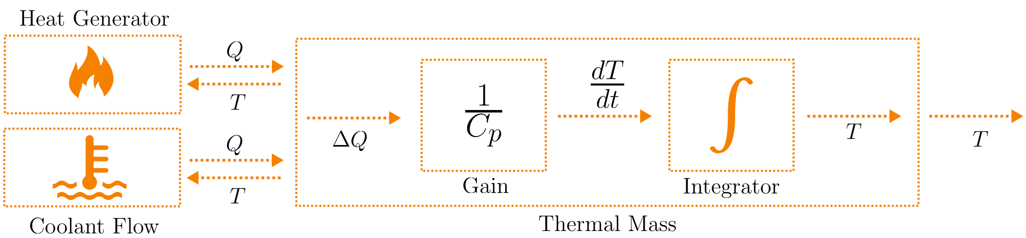

Figure 7. Elements that are modeled to have a finite mass thermally, e.g., fuel cell, electric machine, battery pack, and power electronics, are modeled using the first thermodynamic law using the heat balance and the heat capacity to determine the temperature rise. C_p is the component heat capacity.

In contrast to the fluid dynamic models in the gas exchange systems, incompressibility assumptions are used throughout the cooling system for both air and coolant. Flow through component models either heats or cools the fluid, which alters the outlet temperature. Simple pressure drop equations are used to calculate pressure loss through the component. Flow-splitting devices, such as valves, require a flow-split fraction as input. The split fraction is calculated at the point of confluence and is controlled to equalize pressures in each fluid path as shown in Figure 8. The technique is used for both radiator air and coolant flows and allows for signal flow in one direction.

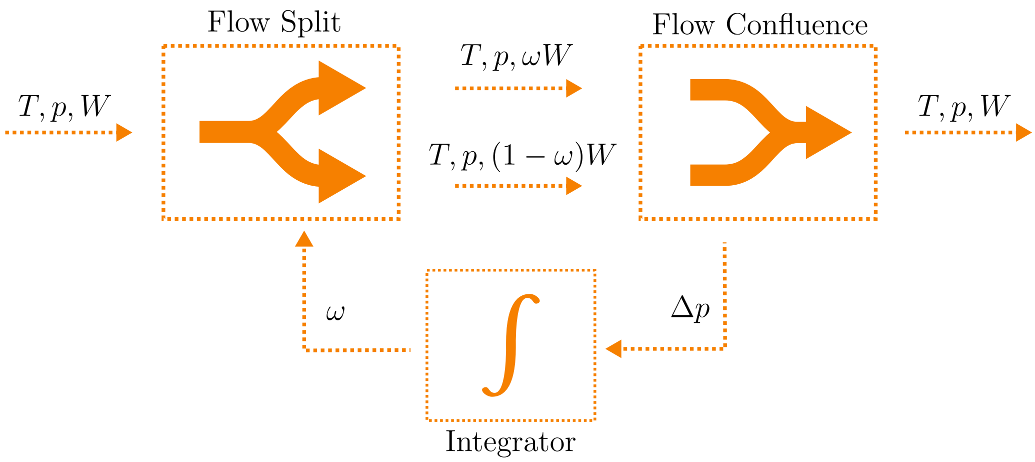

Figure 8. Illustration of how flow-splits are modeled and implemented using the pressure signals and flows to achieve coherence between mass flow splits and pressure gradients in the coolant flow loops.

3.1.6. Control

The control category consists of basic implementations of control algorithms and feedforward calculations that are used to achieve the desirable operating points of the system components. These depend on the case that is run and will be described later in this work.

4. Vehicle System Example Models

The capabilities of the library are presented and illustrated using six examples of vehicle models with increasing levels of technical complexity. Each example builds upon its predecessors according to the hierarchy shown in Figure 9, and for each example, an analysis is performed by varying some model parameter or configuration, in order to illustrate the effects of energy flows, fuel consumption, or other performance indicators.

In this section, the example vehicle models are introduced. A summary of the model parameters is shown in Table 2. This section introduces the example models, while Section 5 discusses the results and the performance.

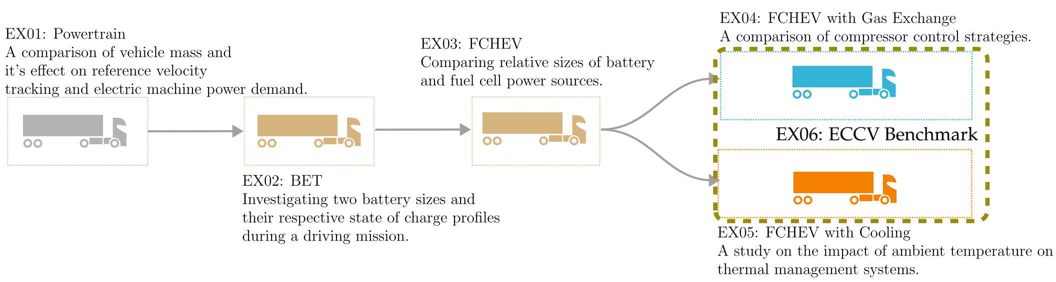

Figure 9. The six examples of vehicle system models. Each example builds on a previous example by adding more components and complexity. The final example Ex. 6, which is the union of Ex. 4 and Ex. 5, was released as the system model for a control benchmark problem.

Table 2. A selection of parameters used in the example vehicle models, highlighting the increase in complexity between models.

Parameter	Ex. 1	Ex. 2	Ex. 3	Ex. 4	Ex. 5	Unit
Mass	20/40	40	40	40	40	ton
EM Rated Power	360	360	360	360	360	kW
Speed Ref.	75	75	75	75	75	km/h
Bus Voltage Ref.		700	700	700	700	V
Bat. Capacity		450/900	360/180	360	360	Ah
Bat. Max. Current		1	1	1	1	C
Conv. Efficiency		0.99	0.99	0.99	0.99	
FC. Stack Power			240/480	240	240	kW
FC. Max. Current			600	600	600	A
FC. Pressure Ref.			2.5	2.5/3.5	2.5	bar
SOC. Ref.			50	50	50	%
Cath. Stoich. Ref.				2		
Amb. Temp.				20	20/40	°C
FC. Mass					72	kg
FC. Heat Capacity					420	J/K
Coolant Flow					4	kg/s
Radiator Area					1	m^2
Radiator Depth					52	mm

4.1. Example 1: Chassis and Powertrain

A signal flow chart of the first example is shown in Figure 10, and its corresponding Simulink implementation is shown in Figures A4 and A5.

As a case study, the vehicle mass is increased from 20 to 40 tons, and the impact on velocity reference tracking and motor power is considered. The driver model is a simple PI controller that tracks a constant reference speed of 75 km/h, and the gear selection depends only on velocity.

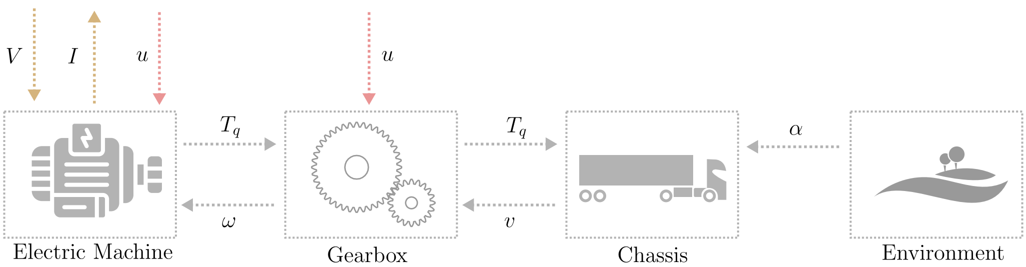

Figure 10. Signal flow of Example 1. Inputs are a torque demand to the electric machine (EM) and a gear selection to the gearbox. The electric machine produces a torque, which is transferred through the gearbox to the wheel. The vehicle acceleration is governed by a force balance between the tractive force and driving resistance forces acting on the chassis. The dominant resistive load is the gravitational force, which acts on the vehicle according to the road slope.

4.2. Example 2: Battery Electric Truck

The second example vehicle aims to demonstrate the battery and power electronics models. A signal flow chart of the battery electric truck powertrain is shown in Figure 11, in addition to the flowchart described for Example 1 in Figure 10. The simulink implementation of Example 2 is shown in Figure A6. The battery current is an input to the system, and it is controlled such that the bus voltage tracks a constant reference. A DC converter boosts the battery voltage to the bus voltage level, and the capacitor acts as a buffer for the DC-bus voltage during power transients, when the electric machine consumes or produces current from the DC-bus.

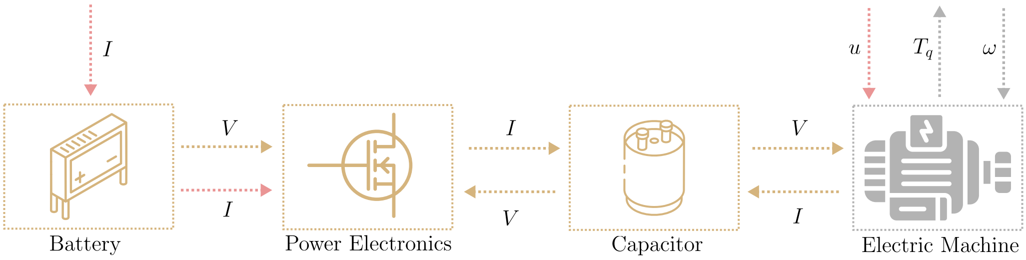

Figure 11. Signal flow chart for the scenario in Example 2. The vehicle model from Ex. 1 is extended by adding a battery, where the battery size is varied between 450 and 900 kWh.

As a case study, two battery sizes, 450 and 900 Ah, and their effects on bus voltage tracking and range are considered. A PI-controller from the control library adjusts the battery current to maintain a DC-bus voltage of 700 V.

4.3. Example 3: FCHEV

In this vehicle model, a fuel-cell system and burn-off resistor are added to Example 2, and the battery size is decreased. A signal flowchart of Example 3 is shown in Figure 12. The battery branch of the electrical network is identical to Figure 11, but a fuel-cell system and burn-off resistor are included on separate branches. The battery, fuel cell, and burn-off resistor are inputs to the model, and they must work together to maintain the DC-bus voltage. A perfect pressure source, which is constant at 2.5 bar, supplies the fuel cell with reactants.

The reduced battery size leads to lower current limits, so a burn-off resistor is included to dissipate energy when the recuperative power exceeds the battery current limit, which typically occurs during steep downhill driving for large vehicles.

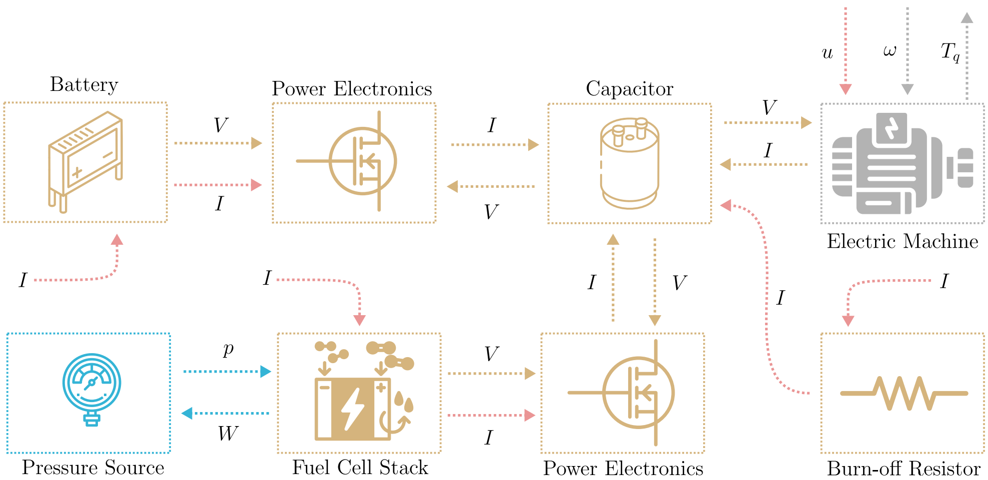

Figure 12. Signal flow of Example 3, where a fuel-cell system with stack and power electronics is added to the system. This example illustrates the properties of the electric vehicle if the vehicle is fuel-cell dominant or battery dominant.

The potential power output of the fuel-cell system versus the battery pack determines if the vehicle is battery or fuel-cell dominant. In this case study, two configurations that lie opposite on this spectrum are considered, and the respective battery and FC parameters for each case are shown in Table 2. The multiple power sources introduce degrees of freedom for the control strategy, and the following control law is used for both the battery- and

FC-dominant vehicles. The battery is mainly responsible for keeping the DC-bus voltage at the reference level, while the fuel-cell current is decomposed in two separate terms. The long-range nominal current is adjusted by a PI controller to maintain the battery state of charge at 50%. Short-term adjustments to the nominal current are made by a separate PI controller to aid the battery in maintaining the DC-bus voltage. If the bus voltage is above the reference by 10 volts, another controller activates the burn-off current to dissipate surplus energy on the DC-bus.

4.4. Example 4: FCHEV with Gas Exchange

In the previous example, the air and fuel supplies were assumed to be perfect such that the focus of analysis could be directed toward energy management. In this example, the details of the air and fuel supplies are considered, continuing with the battery-dominant configuration of the previous example.

Several balance of plant (BOP) components are required to provide reactant chemicals to the anode and cathode at appropriate rates. On the anode side, the main component is the ejector, and on the cathode side, the compressor. A signal flowchart of the anode and cathode gas exchange systems is shown in Figures 13 and 14. Fuel is stored at high pressure in the hydrogen tank. The flow from the tank to the primary manifold is an input to the model. The primary manifold is typically pressurized between 5 and 10 bar. Hydrogen flows through the ejector and, by the Venturi effect, draws exhaust gas from the secondary manifold into the supply manifold. The inlet and outlet to the anode chamber are modeled as flow restrictions. The state in the anode chamber volume is given as input to the fuel-cell voltage model. The supply and secondary manifold represent the combined volumes of pipes and hoses from the ejector to the fuel-cell stack.

The compressor draws ambient air from the environment and pressurizes the supply manifold. Compressor speed dynamics is neglected; instead, the compressor speed is an input to the model, and the consumed power related to the compressor performance is taken from the DC bus. The inlet and outlet to the cathode chamber volume are modeled as flow restrictions. The state in the cathode volume is given as input to the fuel-cell voltage model. A throttle is positioned after the return manifold so that pressure in the cathode chamber can be maintained.

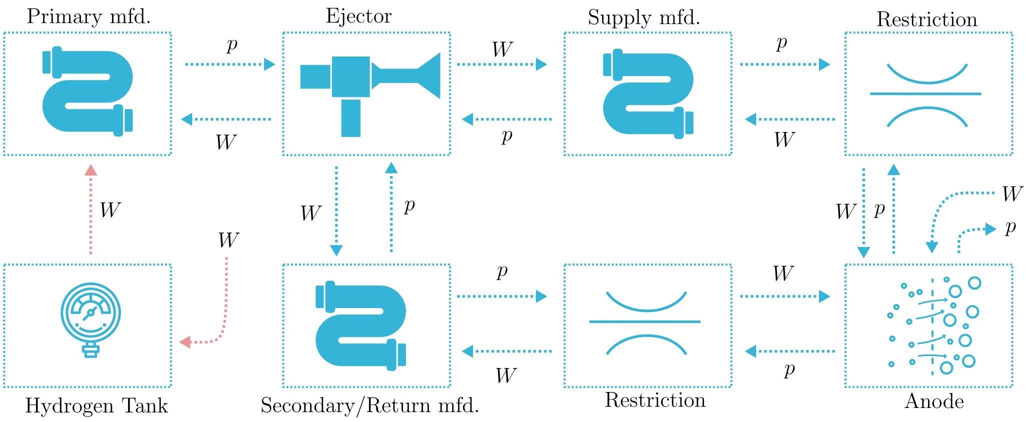

Figure 13. Signal flow of Example 4, anode. In this example, the fuel-cell model is extended with the dynamics of the gas flows through the restrictions and manifolds (mfds) of the fuel cell. The anode is the hydrogen side of the fuel-cell membrane.

In this case study, the compressor and throttle are controlled to track a reference stoichiometry ratio and reference pressure, respectively. The hydrogen flow from the tank to the primary manifold is controlled primarily to provide fuel at the rate of depletion, but adjustments are made to maintain pressure levels similar to the cathode to prevent membrane crossover. The anode stoichiometry is not controlled but is given by the ejector recirculation ratio, and water management is neglected entirely. However, the water produced at the current levels considered in the following case study is enough to sufficiently hydrate the membrane. The ejector performance depends on the pressure ratio between the primary and supply manifold, which in turn depends on the fuel-cell operating point.

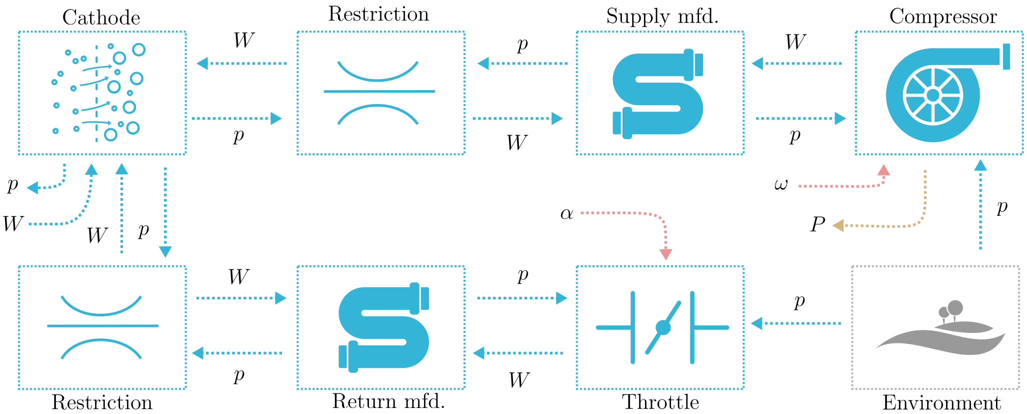

Figure 14. Signal flow of Example 4, cathode. This figure illustrates the components on the air side of the fuel-cell membrane.

As shown in Figure 4, the cell power density increases with pressure. Higher pressure ratios, however, also require more work from the compressor. There is a trade-off between pressure and efficiency, and in this case study, three settings for the reference pressure are considered: 2.5 bar, 3.5 bar, and a dynamic strategy that controls the reference pressure according to the short-term fuel-cell current adjustment explained in the previous example.

4.5. Example 5: FCHEV with Cooling

In Example 3, no BOP systems were considered, and in Example 4, an investigation was made into the challenges of supplying the fuel cell with air and fuel at sufficient rates. Another challenge with fuel-cell systems relates to thermal management. Due to the low operating temperature of 80 °C, the rate of heat transfer from the fuel cell is highly dependent on ambient conditions. In this example, the vehicle model in Example 3 is extended with thermal system models (radiators, thermal inertias, coolant pumps, and fans) in order to illustrate temperature-related effects, and how cooling concerns impact the operation of the vehicle. Signal flowcharts of the thermal systems are shown in Figures 15–17. The chassis and environment models provide speed and ambient conditions to the intake. A dual air stream heat exchanger model, which is described in Figure 17, transfers heat to the air. The relative speed of the fan is an input to the model. The fan creates a pressure increase before the restriction. A restriction model at the flow path outlet determines the flow through the system.

The total coolant flow and initial pressure are inputs to the model. A two-way valve, controlled by an input signal, splits the coolant flow in two paths. One path leads through the fuel-cell stack, and the other through the electric machine, power electronic systems, and the heat exchanger to the battery coolant loop. The flow is combined before the heat exchanger, which transfers coolant heat to the airflow as described in Figure 15.

Air and coolant flow to the heat exchanger as described in Figures 15 and 16. The airflow splits into two paths. One path is through a condenser (typically used for cabin air-conditioning), which heats the air before it reaches the radiator. The second path is through the exposed part of the radiator. The airflow is combined after the radiator, and the split fraction is determined in order to equalize the pressure through each flow path. Coolant flows through the radiator, and the temperature response is delayed based on the height of the radiator. In this case study, the effect of ambient temperature is considered. The coolant pressure, coolant flow, and fan speed are set to constant reference levels, and the coolant valve is controlled to maintain the fuel-cell temperature at 80 or 90 °C.

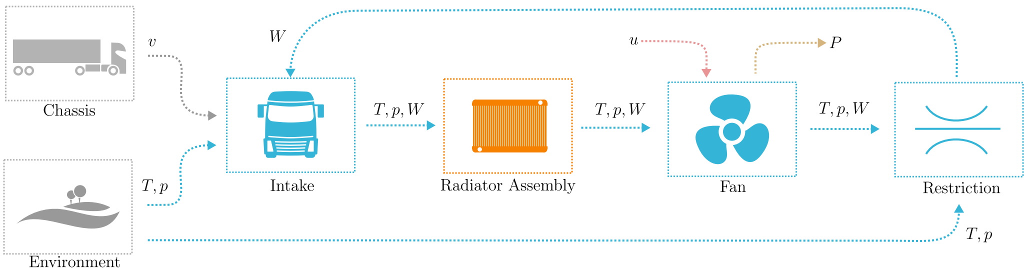

Figure 15. Signal flow of Example 5. Top-level illustration of vehicle and radiator air path, showing how the ambient conditions enter the model and influence the radiator package; this package is described in detail in Figure 16.

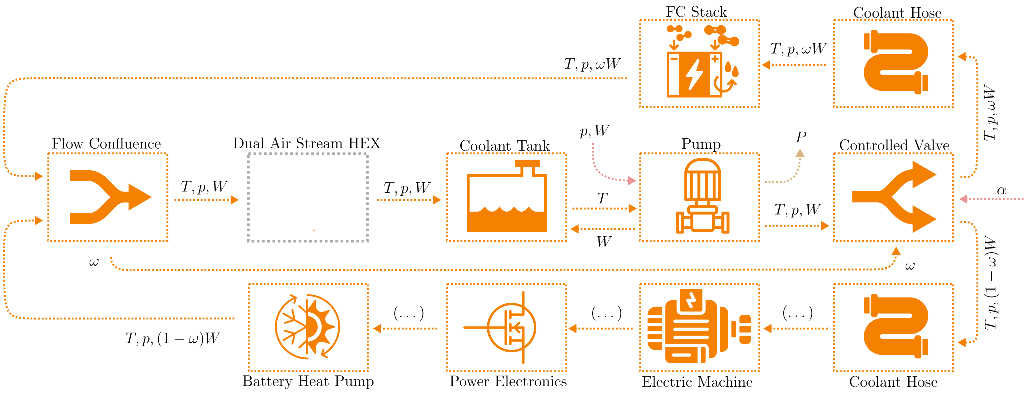

Figure 16. Signal flow of Example 5. Illustration of the coolant loops in the example model. The fuel cell that produces the majority of the heat has its own loop, while the other electric components have a separate loop. The battery also has a heat pump system that maintains its temperature.

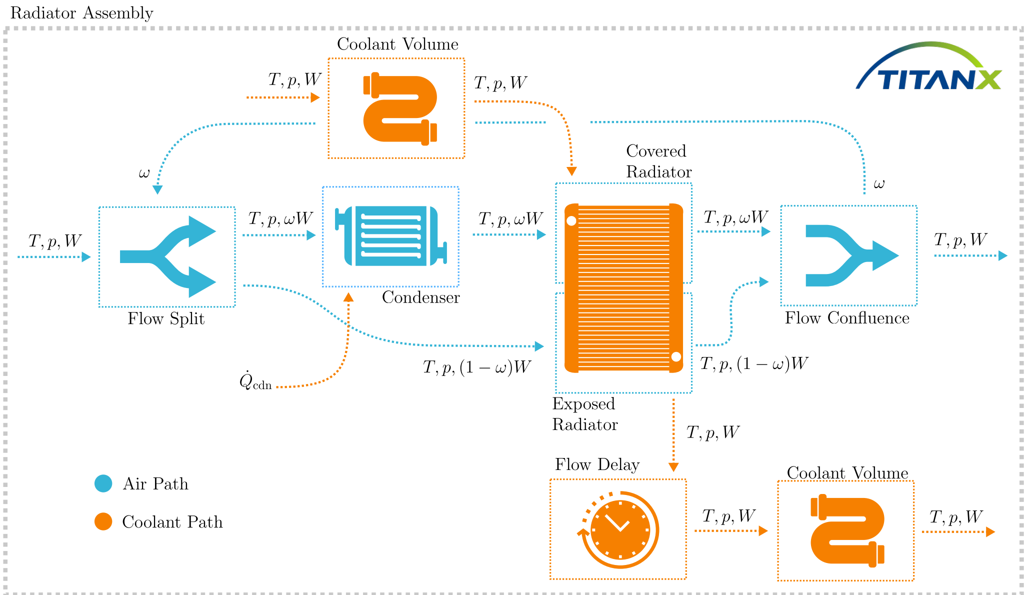

Figure 17. Signal flow of Example 5. Details of the dual air stream heat exchanger that sits in the front of the vehicle.

4.6. Example 6: ECCV Control Benchmark

The last example is the model that was used in the competition IFAC ECCV Control Benchmark for Sustainable Transport. In this example and competition, the balance of plant (BOP) components were included as well as the thermal system, and the contenders had to control the vehicle, the battery, the fuel-cell BOP, and the thermal system. This system is included for completeness here and in the library, providing a reference to a complex system with many control and system design challenges. The benchmark system is intended to act as an inspiration and common ground of comparison for those who want to analyze, learn, and compare variants of the control system. Researchers and students can use this model as a relevant and challenging problem to study and learn about how to control fuel-cell electric vehicles.

5. Results and Discussion

The results for Example 1 are shown in Figure 18. The 20-ton truck is able to follow the velocity reference quite well during the entire mission, while when the 40-ton truck climbs steep hills, its speed is reduced. Analyzing the power of the electric machine, for the 40-ton truck, it is seen that the power (and torque) limit is reached at several points during the mission. In order to improve the speed reference tracking for the 40-ton truck, either the motor power limit needs to be increased, or, a more sophisticated shifting strategy can be implemented.

The results for Example 2 are shown in Figure 19. For the smaller battery, the vehicle does not have enough capacity to complete the mission, but the larger capacity vehicle finishes with approximately 45% remaining. Furthermore, the bus voltage tracking is adequate for the larger battery, while the smaller battery is not able to maintain a constant level. Since the current limit is set to 1 C, the smaller battery cannot produce enough current to maintain the bus voltage during a steep uphill climb.

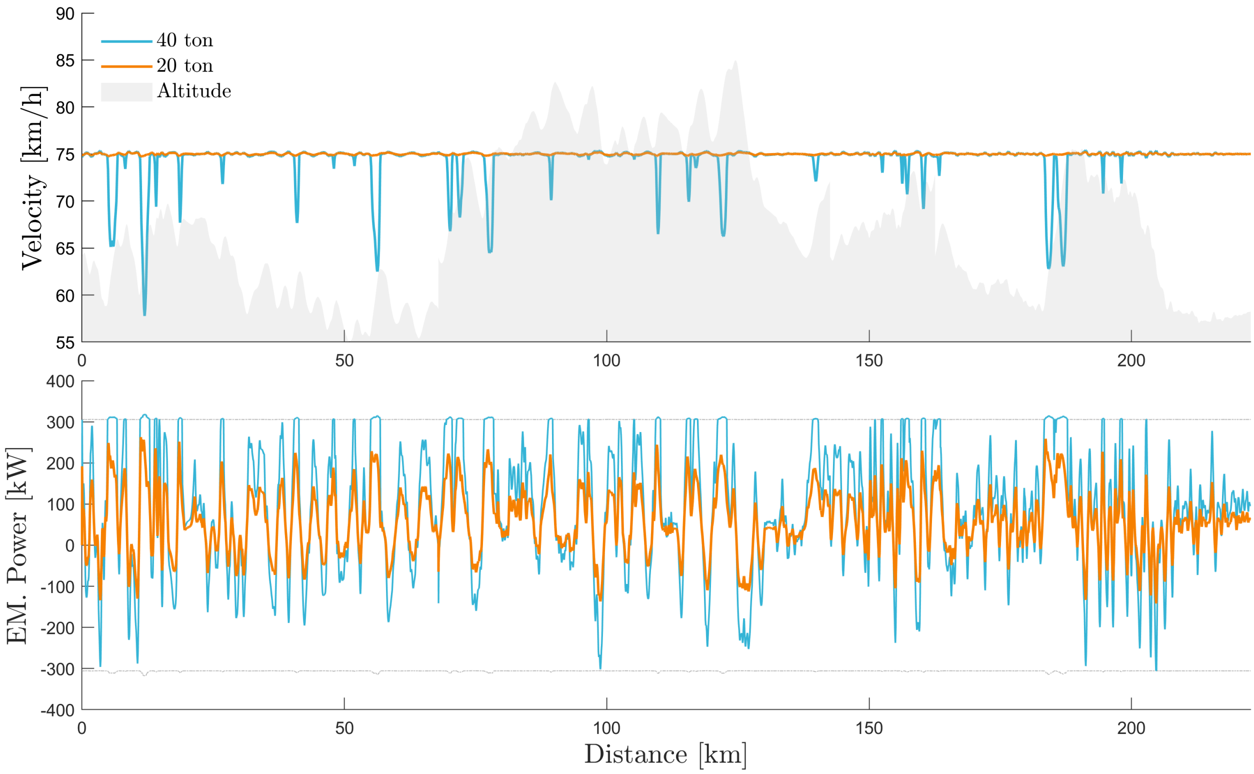

Figure 18. A comparison between two vehicle masses and their effect on velocity reference tracking and motor power. The dotted lines in the lower graph represent the maximum and minimum motor powers at the given speed.

The results for Example 3 are shown in Figure 20. An altitude profile with steep up and down hills is chosen in order to highlight the characteristics of each vehicle configuration. The fuel-cell-dominant vehicle must limit the fuel-cell power output during the second half. Even with a larger battery, the battery-dominant vehicle is required to reduce fuel-cell power output during long downhill segments, and uses the fuel cell for short power boosts uphill.

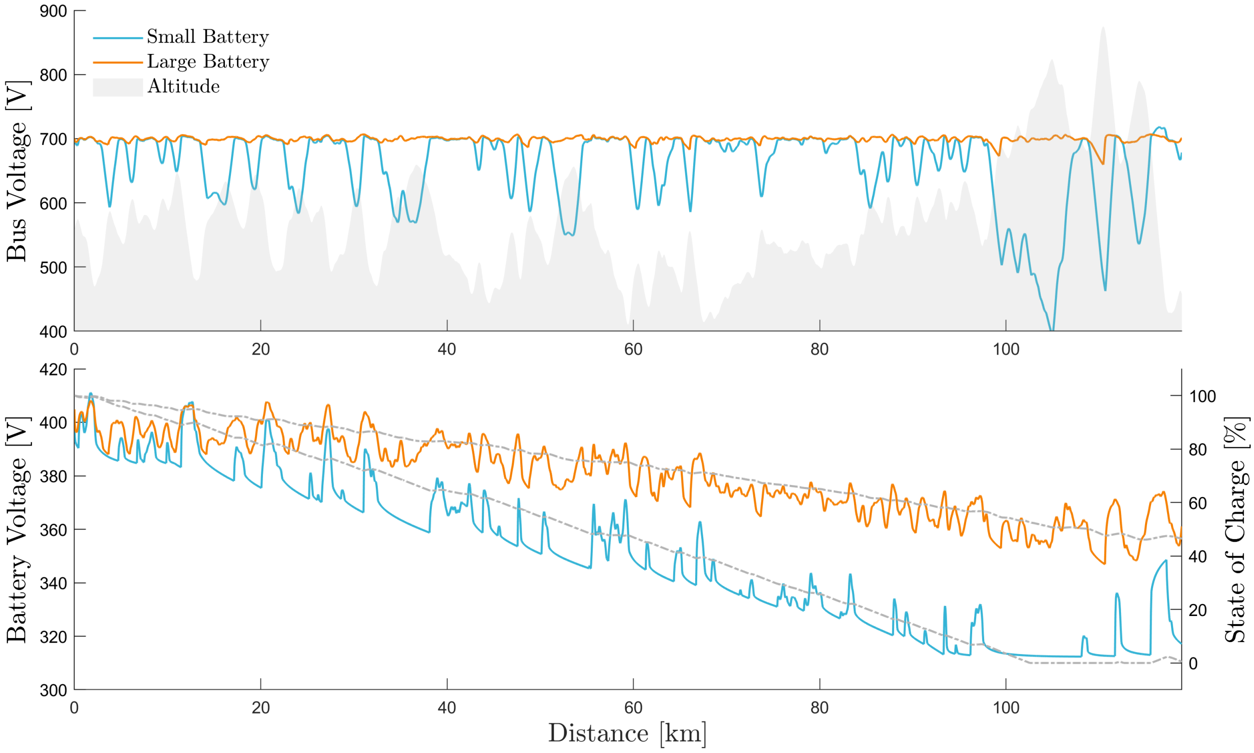

Figure 19. A comparison between battery trucks with small and large battery packs and their impact on range and DC-bus voltage reference tracking. The dotted lines in the lower graph correspond to the state of charge of the respective cases.

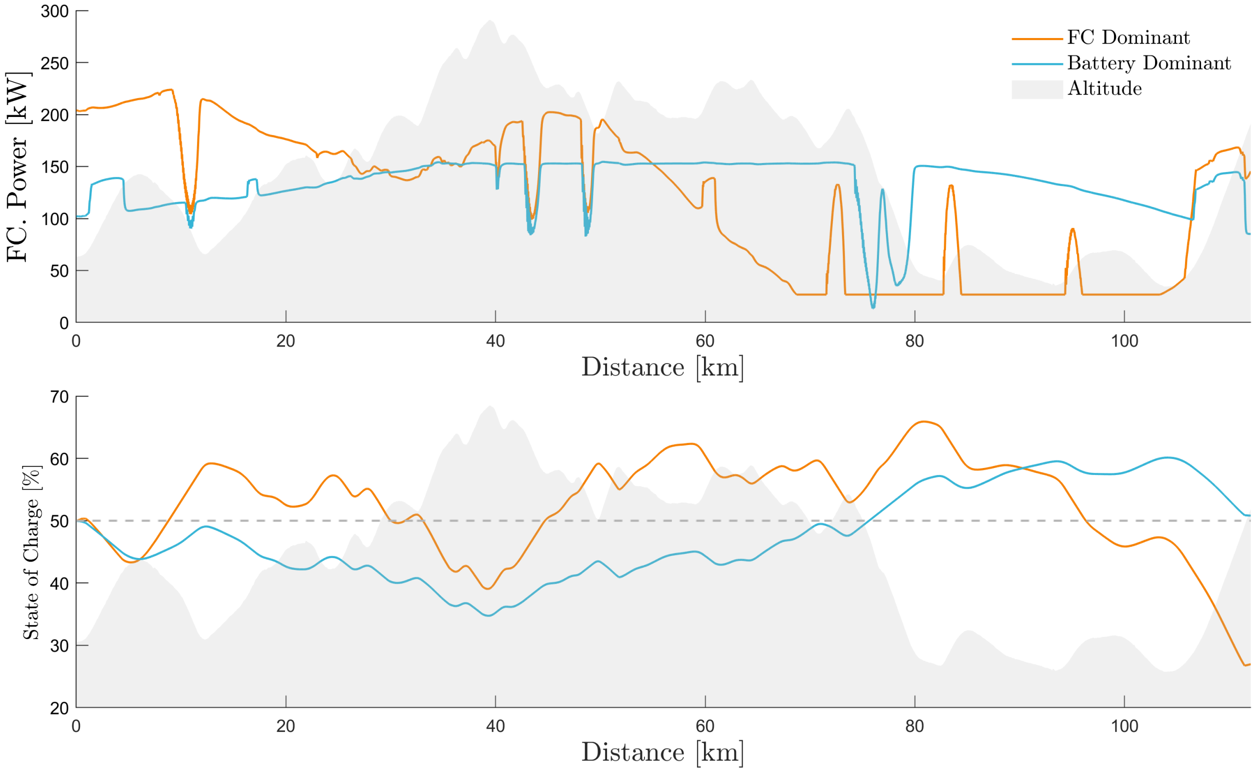

Figure 20. A comparison between battery- and fuel-cell-dominant vehicle configurations, showing the fuel-cell output power and state of charge. The dotted line in the lower graph highlights the 50% reference level.

For Example 4, the results for compressor power demand and anode stoichiometry are shown in Figure 21, for each reference pressure strategy. The compressor power is significantly higher for the high reference pressure setting, while the dynamic strategy ranges between high and low demand, depending on the fuel-cell power output. In Table 3, the fuel consumption for each strategy is given, and it is shown that the benefits in fuel-cell efficiency offset the higher power demand for compression. On the other hand, the recirculation performance is worse for the high-pressure strategy as shown in Figure 21, which may lead to flooding or other issues. A redesign of the ejector, or the inclusion of a hydrogen pump, is needed to increase the recirculation performance of the anode.

Table 3. Fuel consumed using three pressure control strategies.

Pressure	Low	Dynamic	High	
Pressure reference	2.5		3.5	bar
Fuel Consumption	13.00	12.89	12.57	kg

The dynamic pressure reference strategy is designed to increase the concentration of reactants in the anode and cathode during high-load operation. Initially, if only the total pressure is considered it seems that the strategy is successful, as shown in Figure 22. The total pressure in the cathode increases from the low to the high reference level as the current demand is increased. However, when the throttle closes in order to increase the cathode pressure, oxygen is simultaneously depleted at a higher rate, causing depletion spikes as seen in Figure 22, which may be harmful to the device. This phenomenon shows that pressure control strategies should be designed with care.

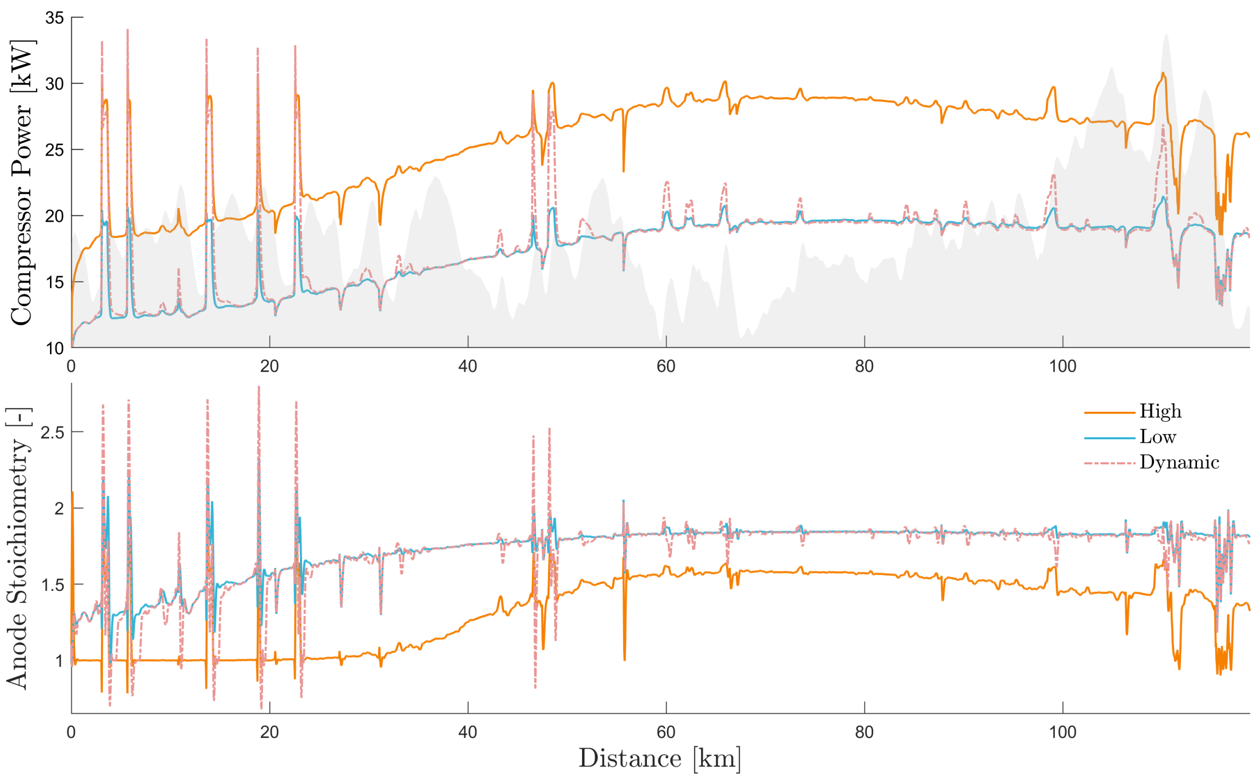

Figure 21. The compressor power demand and anode stoichiometry ratio for three pressure control strategies.

The results for Example 5 are shown in Figure 23. At an ambient temperature of 20 °C, the cooling system maintains FC and EM temperatures at the desired levels. Only late in the driving mission does the fuel-cell temperature-tracking error exceed three degrees.

When the ambient temperature is increased to 40 °C, the radiator's ability to remove heat is drastically reduced. The coolant valve diverts 100% of the flow to the fuel cell, which causes the EM to overheat. If the fuel-cell reference temperature is increased to 90 °C, the temperature difference between the fuel cell and coolant becomes large enough for sufficient heat transfer to occur.

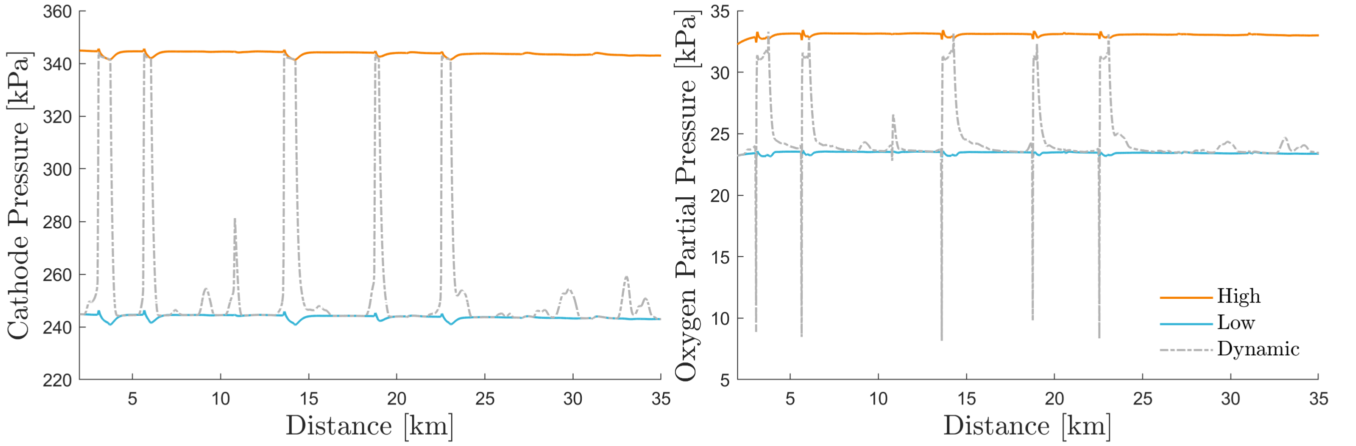

Figure 22. The total cathode pressure and oxygen partial pressure for three pressure control strategies.

High-temperature operation increases cell degradation in low-temperature membranes, and there is increasing interest from industry to investigate medium- to high-temperature fuel-cell membrane technologies. Another way to deal with this issue is to develop smart lookahead controllers that minimize the motor power, and in turn also the fuel-cell heat generation. The ECCV library can aid development in both directions.

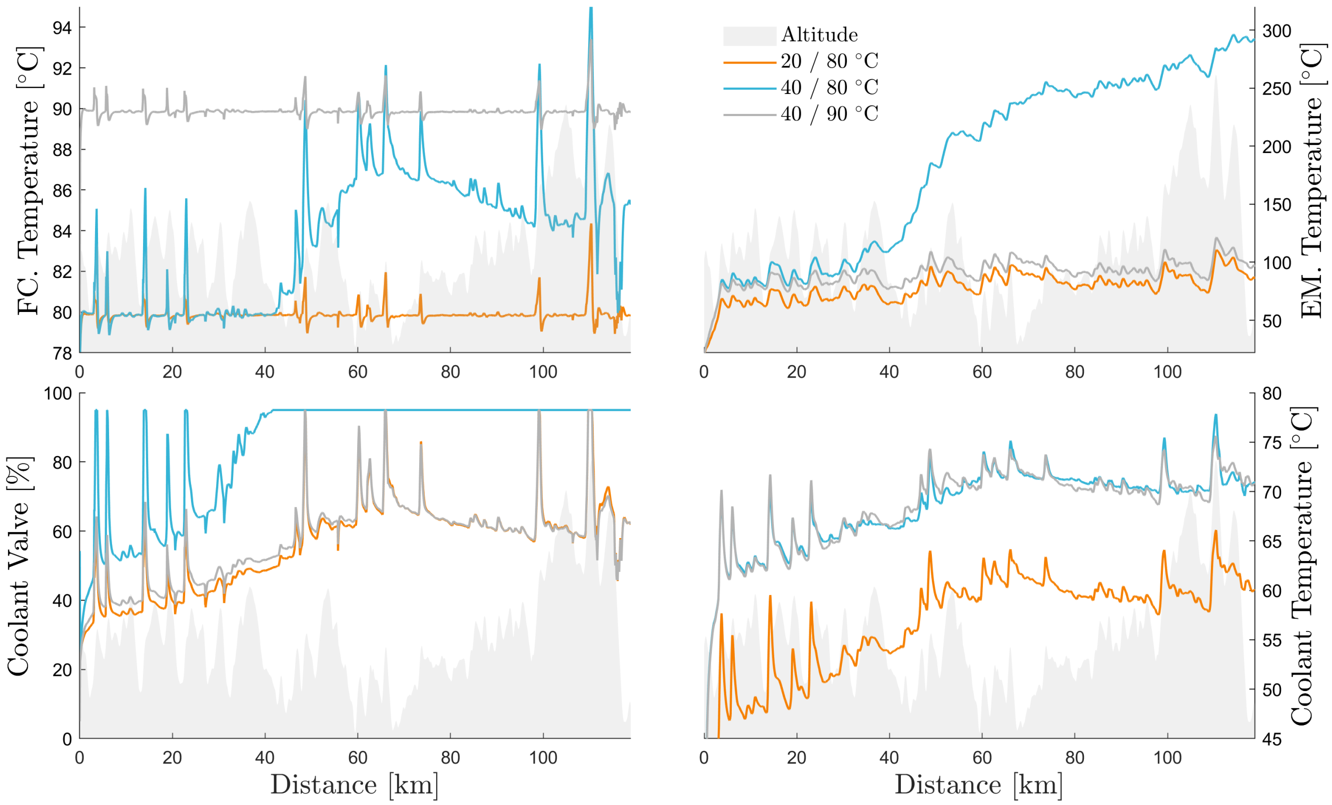

Figure 23. Fuel cell temperature, electric machine temperature, coolant valve position, and coolant temperature results for Example 5.

6. Conclusions

The open-source ECCV platform has been introduced by showing the domains and the foundation for the components, and this was followed by five examples that illustrate the library's capability for vehicle energy analysis. For each of the five vehicle examples, a case study was performed to showcase the analysis capabilities that are enabled by the ECCV platform. The goal of the case studies was also to highlight some of the challenges that heavy-duty FCHEVs are currently facing.

The first case study showed that the ECCV platform can use road altitude profiles to simulate the power demand of heavy-duty vehicles, using standard longitudinal vehicle models. The second case study showed that the platform can be used in the sizing and trade-off calculations between battery size and range. The third case study introduced hybrid vehicle configurations and showed that the platform can be used to determine the relative sizing between the electrochemical power sources, and the development of energy management strategies. The fourth example introduced gas exchange components for the fuel cell and showed that the platform can be used as a tool for the design and control of the balance of plant systems. The fifth example introduced thermal systems and showed that the platform can be used to investigate the thermal performance of cooling layouts and control systems under various ambient conditions. In addition to these five, a sixth example was described and highlighted as a challenging benchmark problem.

The ECCV platform can be downloaded from www.fs.isy.liu.se/Software (accessed on 4 February 2024).

Author Contributions: M.J. is the main developer and author of this paper. A.C. and O.E. developed the radiator models and contributed significantly to the development of the thermal models in general. R.H. and O.L.J. contributed to the model and control development. E.H. contributed with specifications and requirements from the automotive industry side. D.J. and L.E. supervised the research, with L.E. as the project leader. All authors have read and agreed to the published version of the manuscript.

Funding: The work has been funded by The Swedish Energy Agency through The Swedish Electromobility Centre, under project numbers 12034 and 13075.

Data Availability Statement: The ECCV platform is openly accessible and can be downloaded from www.fs.isy.liu.se/Software (accessed on 4 February 2024).

Acknowledgments: Jonatan Siönäs, Daniel Similä, Johannes Wrangstål, Marcus Ögren, Erik Eng, and David Salomonsson are recognized for their master thesis work that contributed to the ECCV platform.

Conflicts of Interest: Authors Arnaud Contet and Olof Erlandsson were employed by the company TitanX. Author Erik Hockerdal was employed by the company Scania. The remaining authors declare that the research was conducted in the absence of any commercial or financial relationships that could be construed as potential conflicts of interest.

Appendix A. Simulink Implementation

This section briefly presents how the ECCV platform is implemented in Matlab Simulink 2023a, including Example 1 and 2.

The ECCV platform integrates well with the industrial toolchain and workflow for analysis and control system development, where code generation from Matlab/Simulink is used to automate the steps from function development to runtime code. To ensure that the ECCV platform models are suitable for control and code generation, only ordinary differential equations are used. Additionally, as illustrated in Figure A1, most models used in the platform are found in a "models"-folder, written as standard Matlab-functions. The ECCV component library is programmatically generated from the function files, and this structure ensures that the same functions used in the platform can be used in a parameter-fitting routine, or any other workflow involving standard Matlab functions.

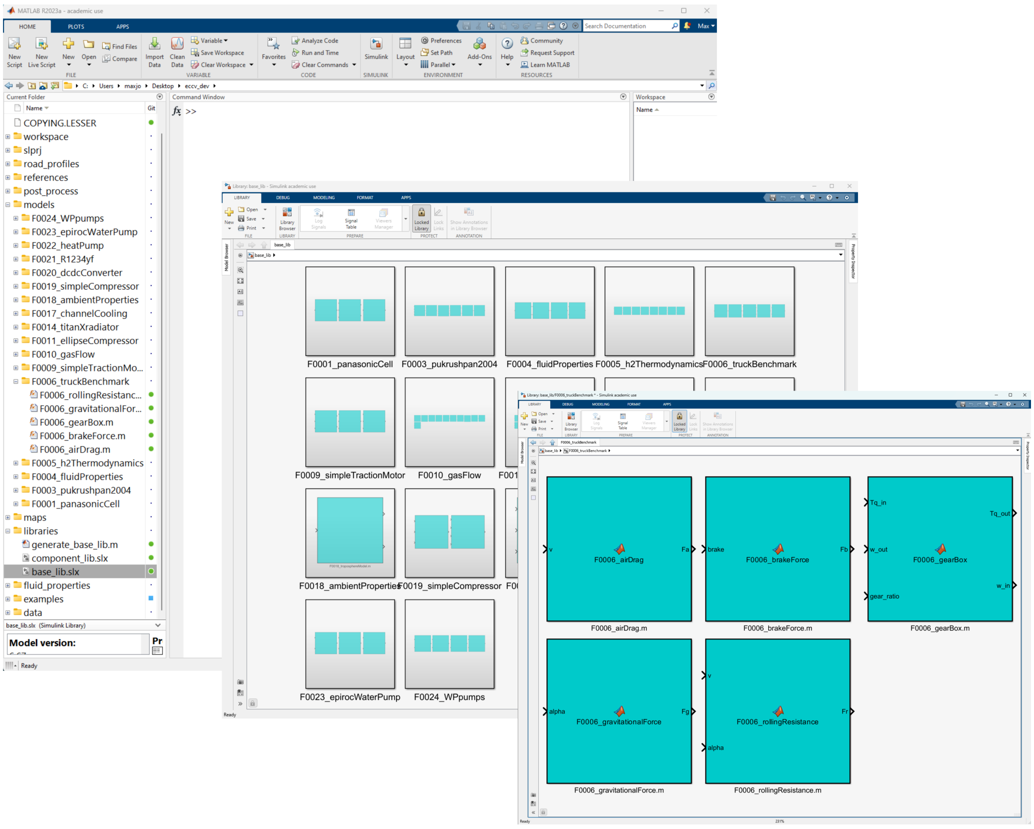

Figure A1. The ECCV base library is shown. The base library is generated programmatically from the models folder, and each subsystem in the library corresponds to an associated model folder. The Matlab functions code is copied into function blocks and can be used to build component models.

The ECCV library is developed for modularity and clean-looking Simulink diagrams, where the interfaces between physical domains are clearly defined. Figure A1 shows the folder structure of the platform. The folder "models" contains additional folders with functions that correspond to a certain component. For example, in Figure A1, the folder "F0006_truckBenchmark" is open. The folder includes the Matlab function file "F0006_airDrag", which is a model for how vehicle velocity generates the driving resistance. A script reads the contents of the "models" folder and updates the Simulink library file "base_lib" accordingly. As shown in the figure, "base_lib" contains subsystems that correspond to each folder in "models". Each subsystem in "base_lib" contains a function-block copy of the corresponding function file. This ensures that the models used in the ECCV platform are defined in a single location, as standard Matlab function files and all simulink implementations are automatically updated by regenerating "base_lib". The function files all comply with Simulink code-generation requirements to enable quick simulation.

Using the function blocks of "base_lib", component models are assembled and sorted into "component_lib", which is shown in Figure A2. The component library is sectioned into four physical domains and two utilities: "Electrochemistry", "Powertrain", "Gas Exchange", "Thermal Systems", "Data and Control", and "Mission". In the figure, the "Electrochemistry" subsystem is open, wherein models for battery, fuel cell, and power electronics are found.

The component models are built using the function blocks from "base_lib" as shown in Figure A3, where a battery cell is modeled as three separate effects that are combined to produce a voltage, given the current, temperature, and state of charge as inputs. The three effects are each represented as separate function blocks: a function for the open circuit voltage "F0001_ocvSOC", a time-domain representation for the Warburg impedance "F0001_dynamicVoltage2", and a maximum-capacity correction based on temperature "F0001_cellCapacity". Modularity is promoted in that users of the platform can substitute any function block with their own implementation, and the function signifier "F000x" ensures that no naming collisions occur.

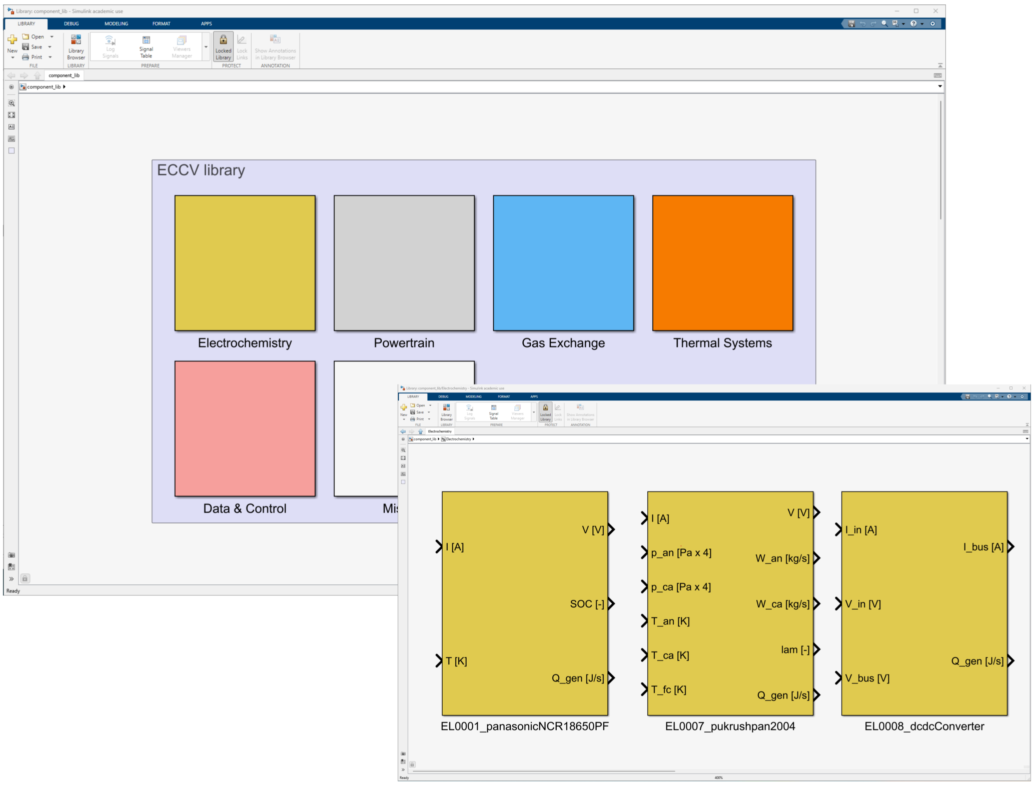

Figure A2. The component library is built using mainly the function blocks from the base library and is sectioned into six categories based on physical domain or functionality.

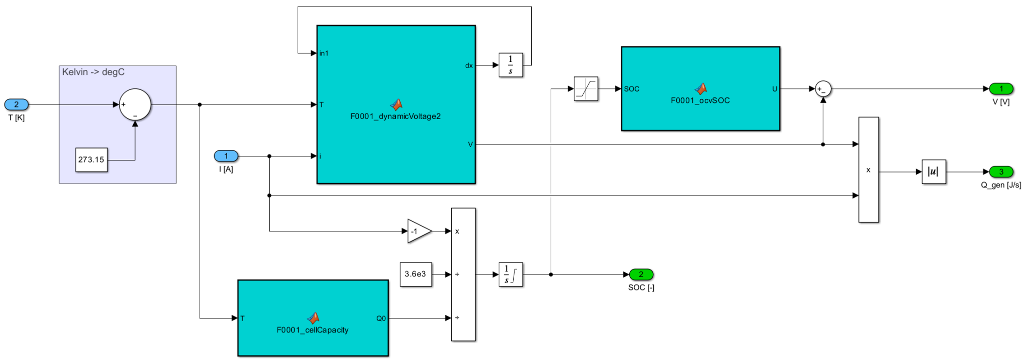

Figure A3. A battery cell voltage model built using the base library functions. Three physical effects (temperature-dependent cell capacity, SOC-dependent open circuit voltage, and internal voltage dynamics) are combined to produce a voltage and heat output.

The ECCV implementation of Example 1 is shown in Figure A4. Driving missions are characterized by the road altitude profile and ambient conditions. In the ECCV platform, velocity is a free variable and depends on how the vehicle is controlled. In Example 1, the velocity is controlled by a simple controller and gear selector. In Figure A4, the "Motor and Gearbox" subsystem has terminated output ports. The terminated ports correspond to the motor current and generated heat, which are used in subsequent examples, but can be ignored if not required.

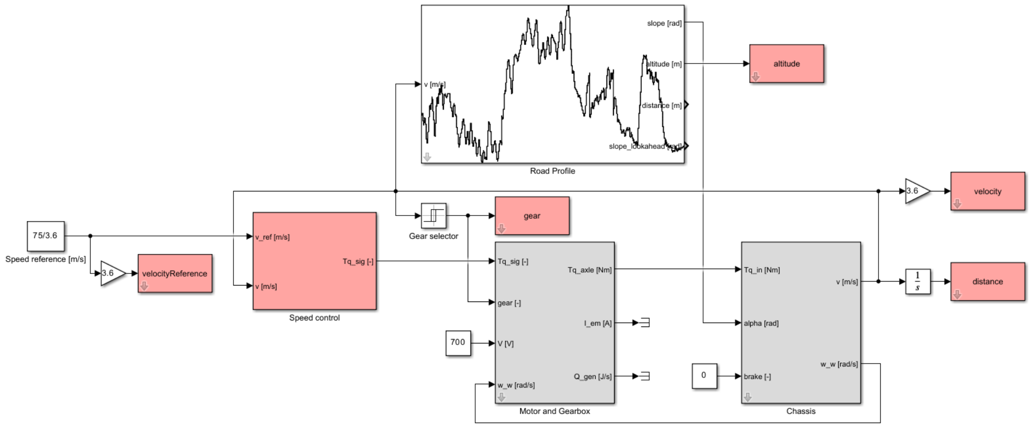

Figure A4. The Simulink implementation of Example 1, which only includes models from the powertrain category of the component library. Altitude and road slope data are available using the road profile block.

The ECCV platform uses the Simulink Data Inspector to visualize and compare signals, and blocks are provided that automatically log signals with a user-specified designator. The data shown in Figure A5 correspond to Example 1. The ECCV platform also provides post-processing scripts to extract data from the Simulink Data Inspector so that standard Matlab graphical tools can be applied.

Figure A5. The Simulink Data Inspector is used to visualize simulation results, and post-processing tools are provided to extract the data to tabular form.

The ECCV implementation of Example 2 is shown in Figure A6. The current draw output port from the motor subsystem is now connected. The net current change is integrated in the capacitor model to produce a DC-bus voltage. Both the motor and DC/DC-converter can be either a producer or a consumer on the bus, and the battery current is controlled to maintain the bus voltage at 700 volts. The implementation of Example 2 is an extension of Example 1, with the inclusion of electrochemical systems, and subsequent examples follow this pattern.

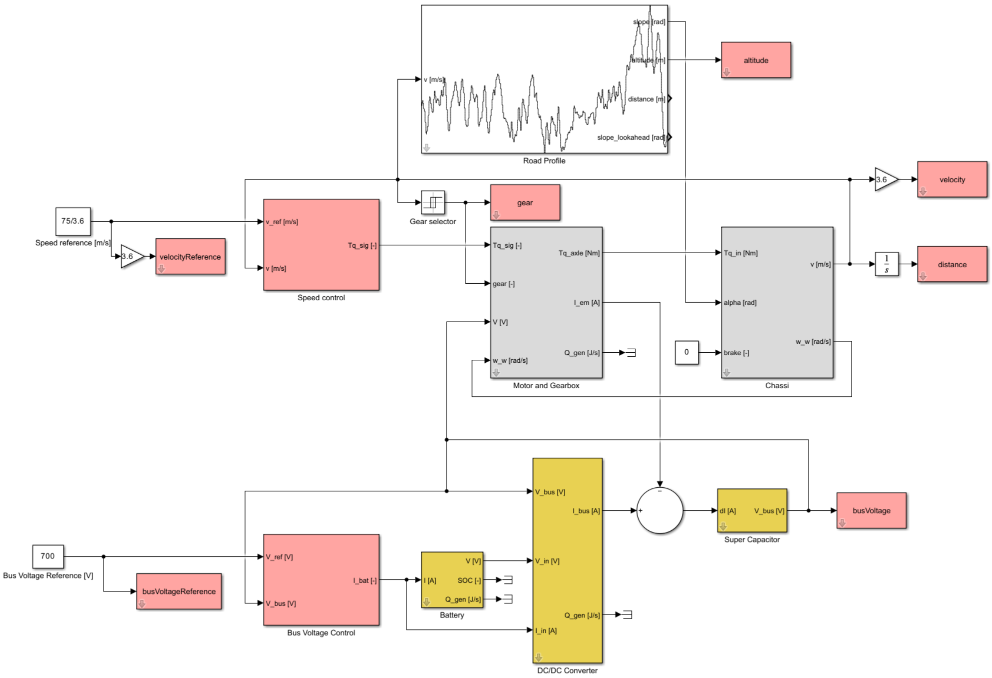

Figure A6. The Simulink implementation of Example 2. The motor and gearbox models are connected to the DC-bus of the electrochemical system.

References

1. Luo, Y.; Wu, Y.; Li, B.; Mo, T.; Li, Y.; Feng, S.P.; Qu, J.; Chu, P.K. Development and application of fuel cells in the automobile industry. *J. Energy Storage* **2021**, *42*, 103124. [CrossRef]
2. Peters, R.; Breuer, J.L.; Decker, M.; Grube, T.; Robinius, M.; Samsun, R.C.; Stolten, D. Future Power Train Solutions for Long-Haul Trucks. *Sustainability* **2021**, *13*, 2225. [CrossRef]
3. Cullen, D.A.; Neyerlin, K.C.; Ahluwalia, R.K.; Mukundan, R.; More, K.L.; Borup, R.L.; Weber, A.Z.; Myers, D.J.; Kusoglu, A. New roads and challenges for fuel cells in heavy-duty transportation. *Nat. Energy* **2021**, *6*, 462–474. [CrossRef]
4. Kast, J.; Vijayagopal, R.; Gangloff, J.J.; Marcinkoski, J. Clean commercial transportation: Medium and heavy duty fuel cell electric trucks. *Int. J. Hydrogen Energy* **2017**, *42*, 4508–4517. [CrossRef]
5. Luo, Y.; Wu, Y.; Li, B.; Qu, J.; Feng, S.P.; Chu, P.K. Optimization and cutting-edge design of fuel-cell hybrid electric vehicles. *Int. J. Energy Res.* **2021**, *45*, 18392–18423. Available online: https://onlinelibrary.wiley.com/doi/pdf/10.1002/er.7094 (accessed on 4 February 2024). [CrossRef]
6. Pardhi, S.; Chakraborty, S.; Tran, D.D.; El Baghdadi, M.; Wilkins, S.; Hegazy, O. A Review of Fuel Cell Powertrains for Long-Haul Heavy-Duty Vehicles: Technology, Hydrogen, Energy and Thermal Management Solutions. *Energies* **2022**, *15*, 9557. [CrossRef]
7. Chen, Q.; Zhang, G.; Zhang, X.; Sun, C.; Jiao, K.; Wang, Y. Thermal management of polymer electrolyte membrane fuel cells: A review of cooling methods, material properties, and durability. *Appl. Energy* **2021**, *286*, 116496. [CrossRef]
8. Wu, J.; Yuan, X.Z.; Martin, J.J.; Wang, H.; Zhang, J.; Shen, J.; Wu, S.; Merida, W. A review of PEM fuel cell durability: Degradation mechanisms and mitigation strategies. *J. Power Sources* **2008**, *184*, 104–119. [CrossRef]
9. Yue, M.; Jemei, S.; Gouriveau, R.; Zerhouni, N. Review on health-conscious energy management strategies for fuel cell hybrid electric vehicles: Degradation models and strategies. *Int. J. Hydrogen Energy* **2019**, *44*, 6844–6861. [CrossRef]
10. Alpaslan, E.; Çetinkaya, S.A.; Alpaydın, C.Y.; Korkmaz, S.A.; Karaoğlan, M.U.; Colpan, C.O.; Erginer, K.E.; Gören, A. A review on fuel cell electric vehicle powertrain modeling and simulation. *Energy Sources Part A Recover. Util. Environ. Eff.* **2021**, 1–37. [CrossRef]
11. Lohse-Busch, H.; Stutenberg, K.; Duoba, M.; Liu, X.; Elgowainy, A.; Wang, M.; Wallner, T.; Richard, B.; Christenson, M. Automotive fuel cell stack and system efficiency and fuel consumption based on vehicle testing on a chassis dynamometer at minus 18 degC to positive 35 degC temperatures. *Int. J. Hydrogen Energy* **2020**, *45*, 861–872. [CrossRef]
12. Fischer, T.; Götz, F.; Berg, L.F.; Kollmeier, H.P.; Gauterin, F. Model based Development of a Holistic Thermal Management System for an Electric Car with a High Temperature Fuel Cell Range Extender. In Proceedings of the 11th International Modelica Conference, Versailles, France, 21–23 September 2015; pp. 127–133.
13. Previati, G.; Mastinu, G.; Gobbi, M. Thermal Management of Electrified Vehicles, A Review. *Energies* **2022**, *15*, 1326. [CrossRef]
14. Brooker, A.; Gonder, J.; Wang, L.; Wood, E.; Lopp, S.; Ramroth, L. FASTSim: A Model to Estimate Vehicle Efficiency, Cost and Performance. In Proceedings of the SAE 2015 World Congress & Exhibition, Detroit, MI, USA, 21–23 April 2015. [CrossRef]
15. Gamma Technologies, LLC. GT-SUITE. 2024. Available online: https://www.gtisoft.com/ (accessed on 4 February 2024).

16. Wang, Y.; Li, J.; Tao, Q.; Bargal, M.H.S.; Yu, M.; Yuan, X.; Su, C. Thermal Management System Modeling and Simulation of a Full-Powered Fuel Cell Vehicle. *J. Energy Resour. Technol.* **2019**, *142*, 061304. [CrossRef]
17. Sandrini, G.; Gadola, M.; Chindamo, D. Longitudinal Dynamics Simulation Tool for Hybrid APU and Full Electric Vehicle. *Energies* **2021**, *14*, 1207. [CrossRef]
18. Meyer, J.; Kiss, T.; Chaney, L. A New Automotive Air Conditioning System Simulation Tool Developed in MATLAB/Simulink. *SAE Int. J. Passeng. Cars-Mech. Syst.* **2013**, *6*, 826–840. [CrossRef]
19. Kiss, T.; Lustbader, J. Comparison of the Accuracy and Speed of Transient Mobile A/C System Simulation Models. *SAE Int. J. Passeng. Cars—Mech. Syst.* **2014**, *7*, 739–754. [CrossRef]
20. Kiss, T.; Lustbader, J.; Leighton, D. *Modeling of an Electric Vehicle Thermal Management System in MATLAB/Simulink*; SAE Technical Paper 2015-01-1708; SAE International: Warrendale, PA, USA, 2015. [CrossRef]
21. Titov, G.; Lustbader, J.; Leighton, D.; Kiss, T. *MATLAB/Simulink Framework for Modeling Complex Coolant Flow Configurations of Advanced Automotive Thermal Management Systems*; SAE Technical Paper 2016-01-0230; SAE International: Warrendale, PA, USA, 2016. [CrossRef]
22. Titov, G.; Lustbader, J.A. Modeling Control Strategies and Range Impacts for Electric Vehicle Integrated Thermal Management Systems with MATLAB/Simulink. In Proceedings of the WCX™ 17: SAE World Congress Experience, Detroit, MI, USA, 4–6 March 2017. [CrossRef]
23. Kirpes, B.; Danner, P.; Basmadjian, R.; Meer, H.d.; Becker, C. E-mobility systems architecture: A model-based framework for managing complexity and interoperability. *Energy Inform.* **2019**, *2*, 1–31. [CrossRef]
24. Eriksson, L.; Thomasson, A.; Ekberg, K.; Reig, A.; Eifert, M.; Donatantonio, F.; D'Amato, A.; Arsie, I.; Pianese, C.; Otta, P.; et al. Look-ahead controls of heavy duty trucks on open roads—Six benchmark solutions. *Control Eng. Pract.* **2019**, *83*, 45–66. [CrossRef]
25. Kollmeyer, P.; Hackl, A.; Emadi, A. Li-ion battery model performance for automotive drive cycles with current pulse and EIS parameterization. In Proceedings of the 2017 IEEE Transportation Electrification Conference and Expo (ITEC), Chicago, IL, USA, 22–24 June 2017; pp. 486–492. [CrossRef]
26. Zhang, C.; Jiang, J.; Zhang, L.; Liu, S.; Wang, L.; Loh, P.C. A Generalized SOC-OCV Model for Lithium-Ion Batteries and the SOC Estimation for LNMCO Battery. *Energies* **2016**, *9*, 900. [CrossRef]
27. Kollmeyer, P. Panasonic 18650PF Li-ion Battery Data. *Mendeley Data* **2018**, *V1* [CrossRef]
28. MathWorks. MATLAB System Identification Toolbox. 2024. Available online: https://www.mathworks.com/ (accessed on 4 February 2024).
29. Pukrushpan, J.T.; Peng, H.; Stefanopoulou, A.G. Control-Oriented Modeling and Analysis for Automotive Fuel Cell Systems . *J. Dyn. Syst. Meas. Control* **2004**, *126*, 14–25. [CrossRef]
30. Leufvén, O.; Eriksson, L. A Surge and Choke Capable Compressor Flow Model—Validation and Extrapolation Capability. *Control Eng. Pract.* **2013**, *21*, 1871–1883. [CrossRef]
31. Llamas, X.; Eriksson, L. *LiU CPgui: A Toolbox for Parameterizing Compressor Models*; Linköping University Electronic Press: Linköping, Sweden, 2018.
32. Llamas, X.; Eriksson, L. Parameterizing Compact and Extensible Compressor Models Using Orthogonal Distance Minimization. *J. Eng. Gas Turbines Power* **2016**, *139*, 012601. [CrossRef]
33. Kuo, J.K.; Hsieh, C.Y. Numerical investigation into effects of ejector geometry and operating conditions on hydrogen recirculation ratio in 80 kW PEM fuel cell system. *Energy* **2021**, *233*, 121100. [CrossRef]
34. Wang, X.; Xu, S.; Xing, C. Numerical and experimental investigation on an ejector designed for an 80 kW polymer electrolyte membrane fuel cell stack. *J. Power Sources* **2019**, *415*, 25–32. [CrossRef]
35. Holman, J. *Heat Transfer*, 10th ed.; McGraw-Hill Education: New York, NY, USA, 2010.